Astrocytic chloride is brain state dependent and regulates cortical neuronal activity

Verena Untiet (✉ verena@sund.ku.dk)
University of Copenhagen https://orcid.org/0000-0002-1888-6378
Felix Ralf Michael Beinlich
University of Copenhagen
Peter Kusk
University of Copenhagen
Celia Kjaerby
University of Copenhagen
Mie Andersen
University of Copenhagen https://orcid.org/0000-0002-6978-585X
Natalie Hauglund
University of Copenhagen https://orcid.org/0000-0002-2198-6329
Björn Sigurdsson
University of Copenhagen https://orcid.org/0000-0002-7484-7779
Hajime Hirase
University of Copenhagen https://orcid.org/0000-0003-3806-6905
Nicolas Petersen
University of Copenhagen https://orcid.org/0000-0001-6206-8295
Alexei Verkhratsky
The University of Manchester https://orcid.org/0000-0003-2592-9898
Maiken Nedergaard
University of Copenhagen https://orcid.org/0000-0001-6502-6031

Article

Keywords:

Posted Date: February 25th, 2022

DOI: https://doi.org/10.21203/rs.3.rs-1364562/v1

Astrocytic chloride is brain state dependent and regulates cortical neuronal activity

Verena Untiet[1*], Felix Beinlich[1], Peter Kusk[1], Celia Kjaerby[1], Mie Andersen[1], Natalie Hauglund[1], Björn Sigurdsson[1], Hajime Hirase[1], Nicolas Caesar Petersen[1], Alexei Verkhratsky[1,3,4], Maiken Nedergaard[1,2*]

[1]Division of Glial Disease and Therapeutics, Center for Translational Neuromedicine, University of Copenhagen, 2200 Copenhagen, Denmark.

[2]Division of Glial Disease and Therapeutics, Center for Translational Neuromedicine, Department of Neurosurgery, University of Rochester Medical Center, Rochester, NY 14642, USA.

[3]Faculty of Biology, Medicine and Health, The University of Manchester, Manchester, M13 9PT, UK

[4]Achucarro Centre for Neuroscience, IKERBASQUE, Basque Foundation for Science, 48011, Bilbao, Spain

* Corresponding authors: Maiken Nedergaard (nedergaard@sund.ku.dk)

Alexei Verkhratsky alexej.verkhratsky@manchester.ac.uk

Verena Untiet (verena@sund.ku.dk)

Abstract

Information transfer within neuronal circuits depends on the balance and recurrent activity of excitatory and inhibitory neurotransmission. Chloride (Cl^-) is the major CNS anion mediating inhibitory neurotransmission[1] and thus essential for balanced brain function. Sustained activation of inhibitory synapses leads to a significant reduction in the amplitude of IPSPs over time, reflecting a collapse of the Cl^- gradient, due to Cl^- influx into neurons through $GABA_A$ receptors[2-4]. Astrocytes are key homeostatic glial cells populating all parts of the central nervous system (CNS)[5]. Despite

astrocytic contribution to brain state transitions, the role of these cells in regulating inhibition remains unexplored. Here we show, for the first time, that astrocytes act as a dynamic Cl^- reservoir regulating Cl^- homeostasis in awake mice. Intracellular chloride concentration ($[Cl^-]_i$) in astrocytes is high and stable during sleep. In awake mice astrocytic $[Cl^-]_i$ is lower and fluctuates in response to both sensory input and motor activity. Stimulation of astrocytic $GABA_A$ receptors induces Cl^- efflux, providing an additional source of Cl^- for inhibitory transmission. Increasing astrocytic $[Cl^-]_i$ by optogenetic manipulations alleviates neuronal activity induced by locomotion or whisker stimulation. Our analysis shows that astrocytes serve as a dynamic source of extracellular Cl^- available for GABAergic transmission in awake mice, which represents a novel mechanism for modulation of the inhibitory tone.

Introduction

Maintaining the balance between excitation and inhibition within a narrow range is critical for proper brain function. To sustain the activity of neuronal networks in time and space, glutamatergic excitation is counteracted by the GABAergic inhibition. Neuronal activity in different brain states is controlled by neurotransmitters, neuromodulators and non-synaptic mechanisms operating at a slower timescale[6,7,8]. In particular, ionic composition of the extracellular space has been identified as a powerful regulator: changing extracellular ion concentration can bypass neuromodulator signalling and directly alter EEG and behavioural state[9,10]. Cortex-wide increases in extracellular $[K^+]_o$ accompany transition from quiet wakefulness to locomotion, while artificial elevation of $[K^+]_o$ enhances spiking and improves motor performance[11]. Sleep duration and sleep architecture are profoundly influenced by fluctuations in $[K^+]_o$[12-15], reflecting the role of $[K^+]_o$ in modulation of neuronal membrane potential, excitability, spiking and oscillatory activity[16-25]. During sleep an increase in $[K^+]_o$ is paralleled by decreases in $[Ca^{2+}]_o$, $[Mg^{2+}]_o$, and $[H^+]_o$, accompanied with shrinkage of the interstitial space[9]. Brain state-dependent regulation of extracellular anions remains,

however, unknown. Inhibitory transmission is mediated by Cl^- fluxes driven by the electrochemical transmembrane Cl^- gradient. Cytosolic Cl^- concentration $[Cl^-]_i$ in neurones is low (~5 mM) but rises rapidly following bursts of GABAergic synaptic activity[3,26]. In the adult brain, astrocytes are believed to maintain, during rest, a high $[Cl^-]_i$ in the range of 20 - 40 mM[27-34], while $[Cl^-]_o$ is about 130 mM, thus setting Cl^- equilibrium potential (E_{Cl}) at ~ -35 mV. The resting membrane potential of astrocytes is ~-80 mV and hence opening of astrocytic $GABA_A$ receptors ($GABA_AR$), generates Cl^- efflux and depolarisation[29,35,36,37]. It has been suggested, but never proven, that efflux of Cl^- from astrocytes may replenish $[Cl^-]_o$ at inhibitory synapses thereby supporting GABAergic transmission[36,37]. Pharmacological blockade of astrocytic gap junctions in brain slices resulted in collapse of inhibitory transmission, supporting the notion that the astrocytic syncytium may serve as a source of Cl^-[38]. However, it remains unknown whether the *ex vivo* preparations accurately replicate astrocytic $[Cl^-]_i$ *in vivo* and how brain state controls astrocytic $[Cl^-]_i$. Here we demonstrate that astrocytic $[Cl^-]_i$ in awake behaving mice is high but changes dynamically along with neuronal activity. Optogenetic manipulations that increase astrocytic $[Cl^-]_i$ potentiate inhibitory transmission. Thus, astrocytes functions as a reservoir of Cl^- for GABAergic transmission thus contributing to the inhibitory tone. These observations may have significant implication for diseases characterized by failure of inhibitory transmission, such as seizures activity.

Results

Astrocytic $[Cl^-]_i$ changes rapidly in response to arousal

To monitor dynamic changes in astrocytic $[Cl^-]_i$ in awake freely moving or naturally sleeping mice, we used fibre-photometry of astrocytes specifically expressing the fluorescent Cl^- sensor mClY under *Gfap*-promoter to record the bulk signal from many cells. mCIY was virally delivered to somatosensory cortex and an optic fibre was implanted above the injection site (Figure 1A). In

addition, electrodes were implanted for simultaneous EEG/EMG recordings. Two weeks after injection and surgery, the mClY signal was recorded early in the dark phase when the animal is mostly awake. Figure 1 illustrates that astrocytic $[Cl^-]_i$ depends on the state of the brain: $[Cl^-]_i$ exhibited dynamic fluctuations, with high frequency and irregular amplitudes during wakefulness, but stabilized during EEG/EMG-validated NREM sleep (Figure 1B and C). On average $[Cl^-]_i$ was significantly higher during sleep than during wakefulness ($p<0.0001$, Figure D). Transition from sleep to wakefulness was accompanied by a consistent decrease in $[Cl^-]_i$, conversely $[Cl^-]_i$ always increased during transition from wakefulness to sleep (Figure 1E). Analysing multiple state transitions in an individual mouse confirmed that astrocytic $[Cl^-]_i$ directly depends on the brain state ($p = 0.0296$, Figure 1F). The standard deviation of bulk $[Cl^-]_i$ signal (which reflects its fluctuations) was significantly higher during wakefulness compared to sleep ($p = 0.0081$, Figure 1F). Highly significant differences between sleep and wakefulness were demonstrated by comparing the distribution of all traces recorded from several mice ($p<0.001$, Figure 1G). As a negative control we recorded fluorescence of YFP expressed under the *Gfap*-promotor. In contrast to mClY, the average YFP signal did not differ between sleep and wakefulness and state transitions were not accompanied with YFP signal changes (Figure 1H). Of note, mClY is based on YFP, but mClY is pH-independent in the physiological range in contrast to YFP[39] (Supplemental Figure 1). Further analysis demonstrated significant correlation between astrocytic $[Cl^-]_i$ and EMG-based estimates of motor activity. When the animal moves, EMG exhibits the highest standard deviation, while in resting or asleep mice the standard deviation is low. The $[Cl^-]_i$ decreased in parallel with an increase in EMG standard deviation ($p = 0.3$, Figure 1J). Comparing the characteristic EEG power bands during sleep with astrocytic $[Cl^-]_i$ showed no correlation. In contrast, during wakefulness EEG theta power, which is associated with movement[40] significantly correlated with astrocytic $[Cl^-]_i$ (Supplemental Figure 2).

To analyse the impact of spontaneous locomotion on $[Cl^-]_i$, periods of mobile and immobile awake states were scored using the video tracking of the animal during mClY recordings (Figure 1K). When locomotion begins, the biphasic (short increase followed by a prolonged decrease) $[Cl^-]_i$ transient is recorded (Figure 1L). Average astrocytic $[Cl^-]_i$ in individual animals showed higher $[Cl^-]_i$ during immobile versus mobile phases (**p = 0.0096), with no changes in the standard deviation of the signal (Figure 1M). Comparing the distribution of all mClY traces recorded, confirms $[Cl^-]_i$ being higher during immobile phases ($p<0.001$, Figure 1N). The relative change of $[Cl^-]_i$ from sleep to wakefulness is larger compared to the relative change between the rest and mobility ($p=0.0695$, Figure 1O).

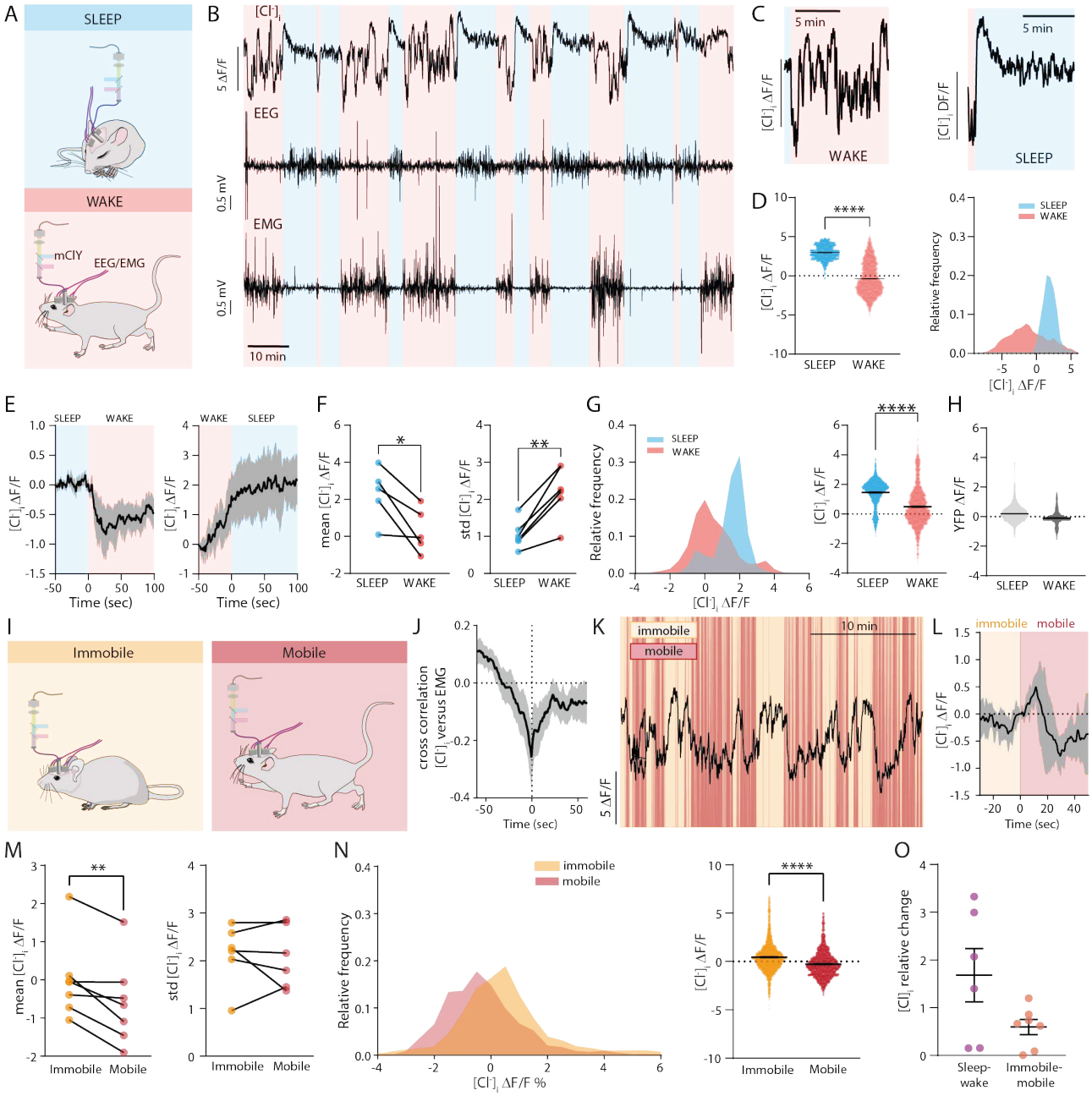

Figure 1: Astrocytic $[Cl^-]_i$ is lower during wakefulness and fluctuates during locomotion.

(A) Experimental protocol: Cortical astrocytic $[Cl^-]_i$ was imaged using mClY and fibre photometry in combination with EEG/EMG recordings in awake, freely moving, or spontaneously sleeping mice. (B) Representative trace of astrocytic $[Cl^-]_i$, EEG, and EMG; colour code indicates sleep and awake periods. (C): Changes in $[Cl^-]_i$ during transiting from sleep to awake or from awake to sleep in expanded time scale. (D) Distribution of astrocytic $[Cl^-]_i$ during sleep and wakefulness (One

sample t-test, N = 1 mouse). (E) Average $[Cl^-]_i$ traces during transition from sleep to awake or awake to sleep, shading indicates SEM. (N = 6 mice). (F) Mean $[Cl^-]_i$ and standard deviation (SD) during sleep and wakefulness (paired two-tailed t-test, N = 6 mice). (G) Distribution of $[Cl^-]_i$ in awake and sleep states recorded from freely moving and intermittently naturally sleeping mice (One sample t-test, N = 6 mice). (H) Distribution of YFP recorded from freely moving intermittently naturally sleeping mice (N = 3 mice). (J) Cross correlation of $[Cl^-]_i$ versus standard deviation of EMG (N = 6 mice). (K) Representative trace of astrocytic $[Cl^-]_i$, EEG, and EMG; colour code indicates mobile and immobile periods. (L) $[Cl^-]_i$ trace during transition from immobile to mobile, shading indicates SD. (N = 7 mice). (M) $[Cl^-]_i$ and standard deviation (SD) during immobile and mobile periods (paired two-tailed t-test, N = 6-7 mice). (N) Distribution of $[Cl^-]_i$ recorded from awake freely moving intermittently mobile or immobile mice (One sample t-test, N = 6 mice). (O) Relative changes of $[Cl^-]_i$ when transiting between sleep and awake versus immobile and mobile (N = 6-7 mice). paired two-tailed t-test. $[Cl^-]$ = mClY -ΔF/F (%).

Onset of movement and sensory stimulation trigger a decrease in astrocytic $[Cl^-]_i$

We next tested whether astrocytic $[Cl^-]_i$ changes during locomotion movement. We recorded bulk astrocytic $[Cl^-]_i$ from somatosensory cortex of head-fixed mice allowed to run voluntarily on a Styrofoam sphere (Figure 2A). Movements were tracked as front paw displacement while simultaneously recording $[Cl^-]_i$. The Cl^- signal was averaged over 4 - 28 movement onsets (Figure 2B and C). Initiation of movement triggered biphasic $[Cl^-]_i$ response comprising a short increase, followed by a slow, long-lasting decrease (Figure 2D). Such $[Cl^-]_i$ dynamics is similar to that observed in freely running mice (Figure 1L). To test whether sensory stimulation also triggers changes in astrocytic $[Cl^-]_i$, trains of air puffs (30 sec, 5 Hz, 50 ms pulse duration) were delivered to the whiskers while astrocytic $[Cl^-]_i$ was imaged in the ipsilateral barrel cortex (Figure 2E). The Cl^-

signal was averaged over several stimulations (Figure 2F). Whisker-induced astrocytic $[Cl^-]_i$ transients followed the same pattern as those triggered by movement. After a fast transient increase, $[Cl^-]_i$ drops and stays low for the duration of the stimulation (Figure 2G).

Fluctuating astrocytic $[Cl^-]_i$ during locomotion and in response to sensory stimulation suggests that astrocytic $[Cl^-]_i$ is involved in cortical processing of brain activity. Both stimuli trigger a similar response in astrocytic $[Cl^-]_i$ (Figure 2H). The amplitude of initial increase, time to peak, negative dip amplitude, time to dip, slope of dip and the sum of positive and negative changes evoked by locomotion or whisker stimulation were all comparable (Figure 2I).

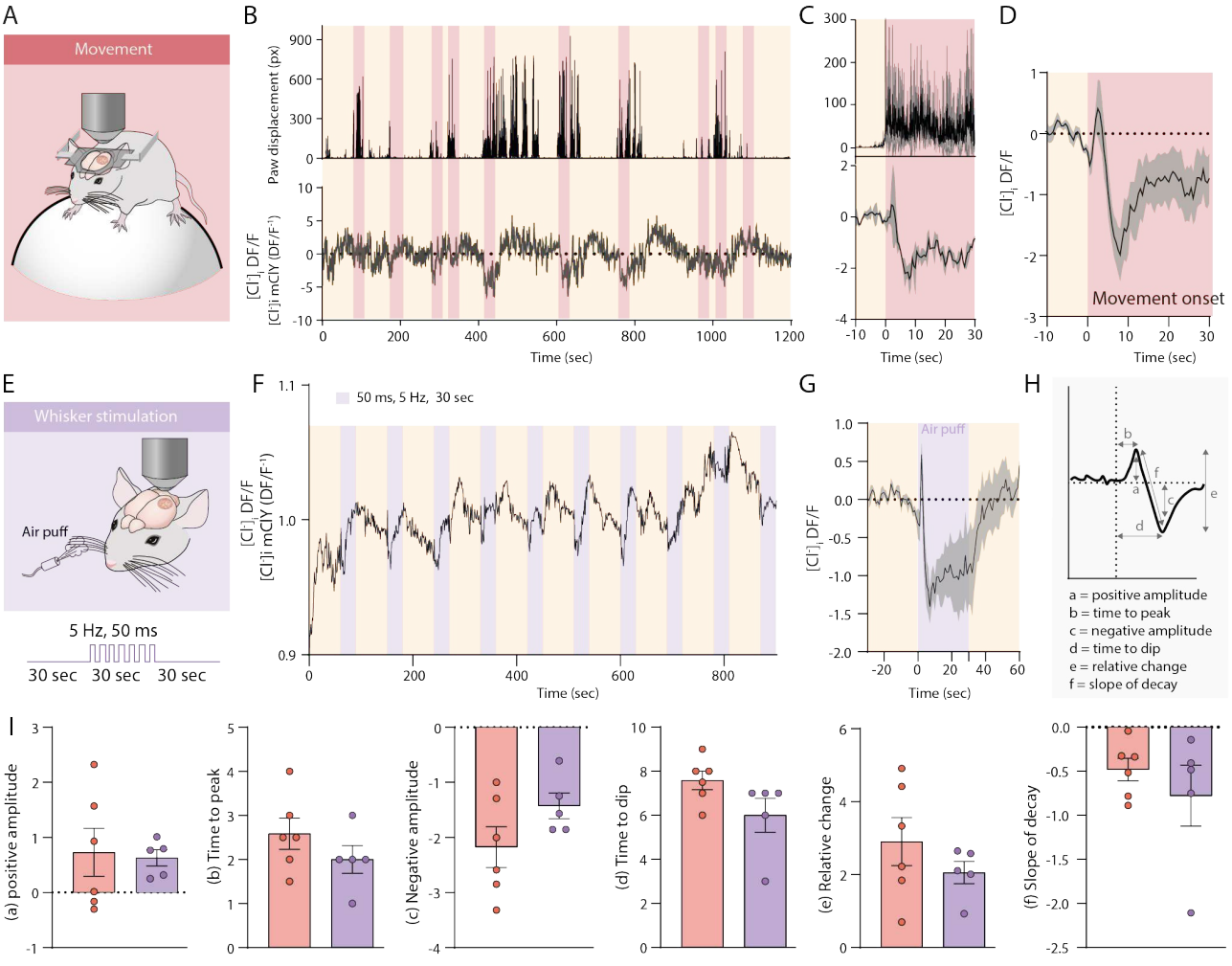

Figure 2: *A*strocytic $[Cl^-]_i$ decreases upon movement and sensory stimulation.

(A) Experimental protocol: Bulk astrocytic $[Cl^-]_i$ was imaged using mClY and macroscopic imaging from somatosensory cortex of awake head-fixed mice voluntarily running on a Styrofoam sphere (B) Representative trace of front paw displacement (top) and astrocytic $[Cl^-]_i$ (bottom). (C) Average of conclusive $[Cl^-]_i$ traces (bottom) of (B) during multiple running periods aligned to the running onset (top). (D) Average $[Cl^-]_i$ trace during movement onset, shading indicates SEM. (N = 6 mice). (E) Experimental protocol: Bulk astrocytic $[Cl^-]_i$ was imaged in somatosensory cortex of awake stationary head-fixed mice subjected to air-puff whisker stimulation. (F) Representative trace of astrocytic $[Cl^-]_i$ upon whisker stimulation (G) Average $[Cl^-]_i$ trace during whisker stimulation, shading indicates SEM. (N = 5 mice). (H) Scheme of Cl^- signal analysis. (I) Comparison of the parameters of the stereotypical astrocytic $[Cl^-]_i$ response to movement versus whisker stimulation depicted in Panel H (un-paired, two-tailed t-test. N = 5-6 mice). $[Cl^-]$ = mClY -ΔF/F (%).

Optogenetic elevation of astrocytic $[Cl^-]_i$ suppresses neuronal activity

To investigate whether manipulations of astrocytic $[Cl^-]_i$ affect neuronal activity, the optogenetic Cl^- pump Halorhodopsin (NpHR3.0) was expressed by injecting AAVs carrying the *Gfap*-NpHR3.0 construct to somatosensory cortex to manipulate $[Cl^-]_i$ in astrocytes (Figure 3A). Neuronal activity was monitored by imaging bulk neuronal $[Ca^{2+}]_i$ using the redshifted Ca^{2+} probe jRGECO1a, expressed by injecting the viral construct *hSyn1*-jRGECO1a, in awake, head-fixed mice voluntarily running on a Styrofoam sphere. Onset of voluntary running evoked an increase in neuronal $[Ca^{2+}]_i$ lasting for the duration of the locomotion (Figure 3B). To manipulate astrocytic $[Cl^-]_i$, which is decreased upon movement onset (Figure 3C), the optogenetic Cl^- pump NpHR3.0 was activated with yellow light (575 nm). Constant stimulation of NpHR3.0 significantly increases astrocytic $[Cl^-]_i$ (Supplemental Figure 3 and 4), while the stimulation light alone, applied to mice not expressing NpHR3.0, affected neither astrocytic $[Cl^-]_i$, nor brain activity (Supplemental Figure 5).

Accumulation of Cl^- into astrocytes by activation of NpHR3.0 modified neuronal Ca^{2+} dynamics. Most notable is the suppressed plateau phase of the neuronal response when NpHR3.0 is activated. While the amplitude and time to peak were not different, the amplitude of the plateau decreased, and the decay of $[Ca^{2+}]_i$ transient accelerated ($p=0.0384$ (Figure 3D). The recovery time to baseline of neuronal $[Ca^{2+}]_i$ was also significantly faster ($p=0.0049$, Figure 3D). Overlaying neuronal $[Ca^{2+}]_i$ and astrocytic $[Cl^-]_i$ transients evoked by onset of locomotion, shows that the suppression of neuronal activity occurs concurrently with the peak of astrocytic Cl^- efflux of (Figure 3C). These data suggest that optogenetic activation of NpHR3.0 counteracts the decrease of astrocytic $[Cl^-]_i$ and thus maintains high $[Cl^-]_i$ during neuronal activation.

To further characterise the impact of astrocytic $[Cl^-]_i$ on neuronal activity, we manipulated astrocytic $[Cl^-]_i$ during whisker puff stimulation. This approach provided temporal control which was lacking when studying spontaneous movement (Figure 3E). Air-puffing onto the whiskers increased neuronal $[Ca^{2+}]_i$ that lasted for the length of the stimulation (Figure 3F). Again, optogenetic stimulation was employed to counteract the decrease of astrocytic $[Cl^-]_i$ upon whisker stimulation (Figure 3G.) Activation of NpHR3.0 in astrocytes decreased the plateau phase and significantly accelerated the decay of neuronal $[Ca^{2+}]_i$ transient (Figure 3H). Neither the amplitude nor the time to peak of neuronal $[Ca^{2+}]_i$ increases were affected by activation of NpHR3.0 in astrocytes (Figure 3H). An overlay (Figure 3G) shows that the largest change in astrocytic $[Cl^-]_i$ occurred 6-8 seconds after the beginning of whisker stimulation. A significant reduction in neuronal $[Ca^{2+}]_i$ occurred concomitantly with the dip in astrocytic $[Cl^-]_i$ (Figure 3H). Light-induced increase in astrocytic $[Cl^-]_i$ consistently decreased the neuronal response to whisker stimulation (Figure 3H). We conclude that manipulations that increases astrocytic $[Cl^-]_i$ dampen prolonged neuronal activity. While the initial timing and the maximal amplitude of neuronal $[Ca^{2+}]_i$ are not changed, elevations of astrocytic $[Cl^-]_i$ have a significant impact on the plateau of the neuronal response and acceerates

recovery to the baseline of neuronal $[Ca^{2+}]_i$ evoked by both spontaneous locomotion and whisker stimulation. Incidentally, allosteric $GABA_AR$ agonist diazepam affects neuronal $[Ca^{2+}]_i$ transient similarly to the activation of NpHR3.0 in astrocytes (Supplemental Figure 6). These findings support the notion that astrocytic $[Cl^-]_i$ serves as an important source of Cl^- for GABAergic transmission. Transient increases in excitatory transmission in awake behaving mic are terminated faster when astrocytic $Cl^-]_I$ is high.

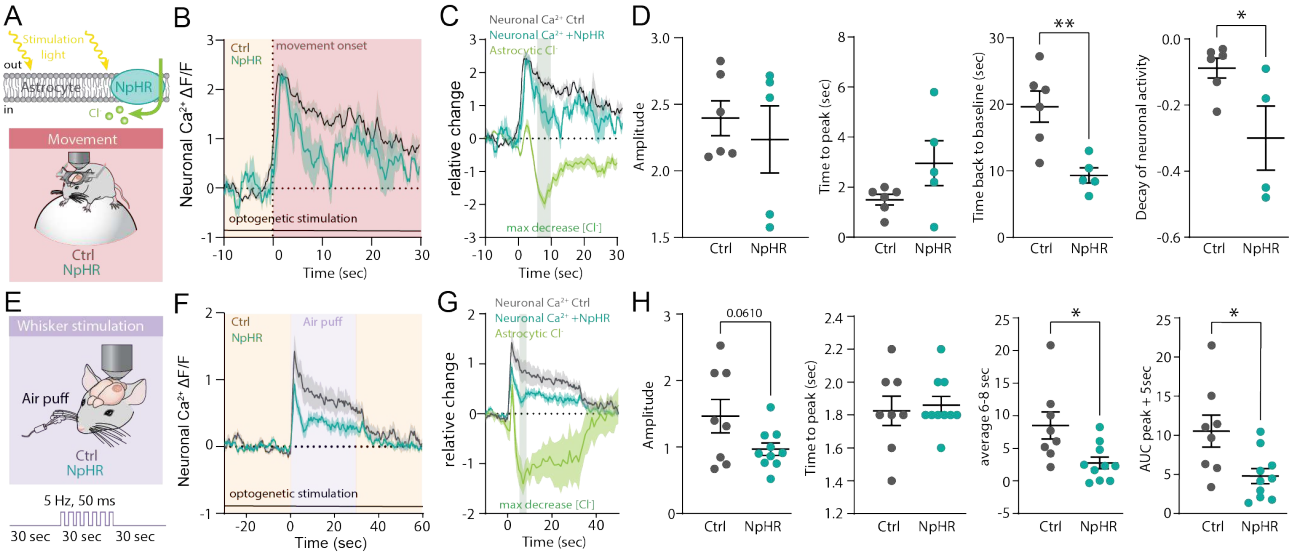

Figure 3: Optogenetic elevation of astrocytic $[Cl^-]_i$ shortens activation-induced neuronal $[Ca^{2+}]_i$. (A) Experimental protocol: The optogenetic Cl^- pump was expressed in astrocytes to manipulate $[Cl^-]_i$, while neuronal $[Ca^{2+}]_i$ was imaged using jRGECO1a. As the negative control light stimulation was applied to mice not expressing NpHR3.0. The awake, head-fixed mice were voluntarily running on a Styrofoam sphere. (B) Average neuronal $[Ca^{2+}]_i$ trace during transition from stationary to mobile, while simultaneously stimulating the optogenetic tool NpHR3.0 in astrocytes, shading indicates SEM. (N = 3 mice). (C) Overlay of neuronal $[Ca^{2+}]_i$ (same as B) and astrocytic $[Cl^-]_i$ (same as Figure 2D) traces during transition from stationary to mobile, shading indicates SEM. (D) Shows maximal (peak) amplitude of neuronal $[Ca^{2+}]_i$ upon movement onset;

time to peak of neuronal Ca^{2+} upon movement onset; recovery time to baseline; slope of decay of $[Ca^{2+}]_i$ transient (N = 5-6 mice).

(E) Using the same protocol as in (A), whiskers were stimulated using air puffs. (F) Average neuronal $[Ca^{2+}]_i$ trace during whisker stimulation in control and upon light-activation of optogenetic tool NpHR3.0 in astrocytes, shading indicates SEM. (N = 8-10 mice). (G) Overlay of neuronal $[Ca^{2+}]_i$ (same as C) and astrocytic $[Cl^-]_i$ (same as Figure 2G) traces during whisker stimulation, shading indicates SEM. (H) Maximal (peak) amplitude of neuronal $[Ca^{2+}]_i$ upon whisker stimulation; time to peak of neuronal $[Ca^{2+}]_i$ upon whisker stimulation. Neuronal $[Ca^{2+}]_i$ during the period of maximal astrocytic $[Cl^-]_i$ changes upon whisker stimulation, 6 – 8 sec after onset of stimulation. Area under the curve (AUC) of neuronal $[Ca^{2+}]_i$ during 5 sec after peak. Un-paired two-tailed t-test.

Activation of $GABA_A$ receptors triggers Cl^- efflux from astrocytes

We tested the hypothesis that activation of $GABA_AR$ in the setting of locomotion and whisker stimulation is responsible for efflux of astrocytic $[Cl^-]_i$ [36-38]. Astrocytes express $GABA_ARs$ which are predominantly localized around inhibitory synapses[41] raising the possibility that GABA activates astrocytic $GABA_ARs$ close to the synaptic cleft thereby supplying Cl^- to sustain inhibitory transmission. To activate $GABA_ARs$, either GABA or the $GABA_AR$ agonist muscimol were applied by pressure injection through a micropipette (500 μM, 1-3 μm tip diameter, 2-8 psi, 100 ms) as described previously[42], while recording fluorescence intensity of mClY or MQAE (Figure 4A). Opening of GABA-gated anion channel leads to Cl^- movement along the diffusion gradient, hence changes in $[Cl^-]_i$ reveal the direction of Cl^- fluxes.

The genetically encoded Cl^- sensor mClY was expressed by injection of AAVs carrying the *Gfap*-mClY construct into somatosensory cortex (Figure 4B). Muscimol induced a transient decrease in $[Cl^-]_i$ in awake animals (Figure 4C) that lasted for 8.36 ± 3.1 seconds (Figure 4D).

This observation was verified by imaging astrocytes loaded with the Cl^- dye MQAE while cell type identity was confirmed by co-labelling with astrocyte-specific dye SR-101[43,44] (Figure 4F). MQAE has been shown before to be insensitive to bicarbonate and pH changes, while mClY is Cl^- selective at physiological pH ranges[39]. Fluorescence intensity as well as fluorescence lifetime directly report the $[Cl^-]_i$. Absolute $[Cl^-]_i$ imaging of fluorescence lifetimes in awake mice *in vivo* shows a normal distribution as reported previously for in brain slices and cell culture[33,34] (Supplemental Figure 3). Imaging MQAE fluorescence intensity was used as an alternative approach to critically test the data based on the genetic Cl^- indicator mClY. Imaging of MQAE revealed that GABA administration reduced $[Cl^-]_i$ corroborating the mCIY data (Figure 4G). The transient decrease of $[Cl^-]_i$ was rapid and lasted for 15.10 ± 10.1 (Figure 4H and I). Muscimol also triggers transient decrease in $[Cl^-]_i$ with an average duration of 14.89 ± 7.6 seconds (N = 10 mice) (Figure 4H and I). As a negative control aCSF was pressure injected through a micropipette with the same settings as used for GABA and muscimol administration. In contrast to muscimol and GABA injections, aCSF produces a fast artefact lasting 1.2 ± 0.73 (N = 1 mouse) seconds and does not affect $[Cl^-]_i$ (Figure 4J, K, and L). These observations show that basal astrocytic $[Cl^-]_i$ *in vivo* is above the diffusion equilibrium of 7 mM Cl^- by which Cl^- channel opening triggers Cl^- efflux.

We can conclude that astrocytes respond to GABA with a decrease in $[Cl^-]_i$ resulting in Cl^- efflux that might be directed into the synaptic cleft based on the high density of GABAA receptors around inhibitory synapses[41]. In this way astrocytes provide a simple mechanism to modulate neuronal inhibition that acts on a global and slower time scale that synaptic transmission itself.

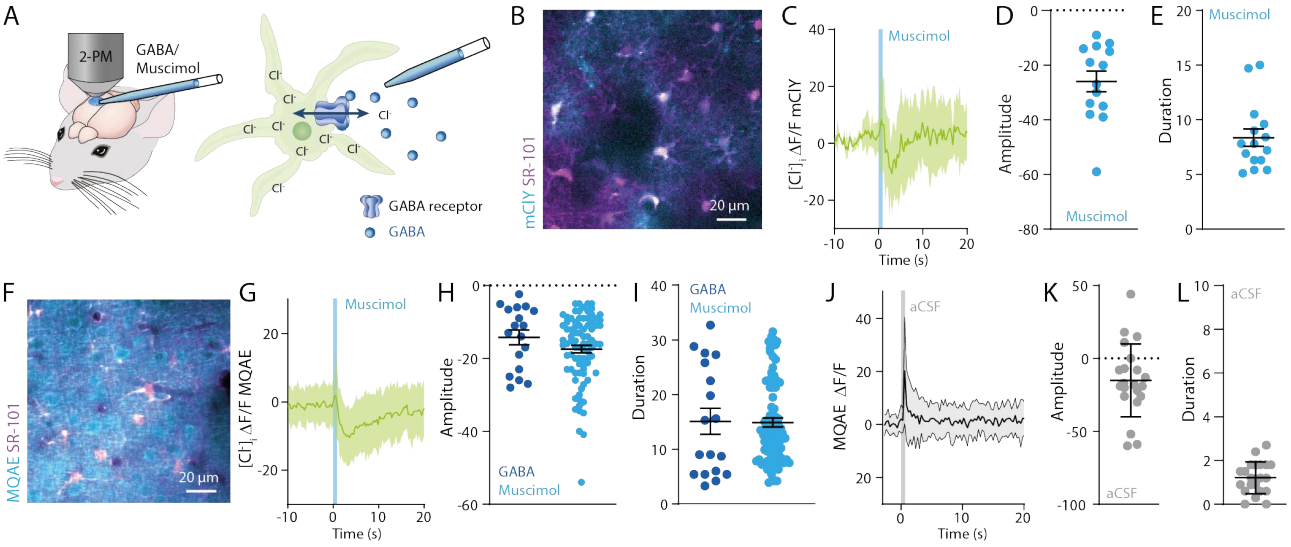

Figure 4: Activation of $GABA_A$ receptors in awake mice, trigger Cl^- efflux from astrocytes.

(A) Experimental protocol: Astrocytic $[Cl^-]_i$ recordings using mClY or MQAE in response to injections of GABA or muscimol. (B and F) Representative images of the mouse cortex expressing mClY in astrocytes or loaded with MQAE and co-labelling with SR-101. (C and G) Astrocytic $[Cl^-]_i$ traces during muscimol injection, shading indicates SD. (N = 3 mice). (D and H) Decrease of astrocytic $[Cl^-]_i$ in response to muscimol or GABA injections, (mean ± SD, N = 3-10 mice). (E and I) Duration of astrocytic $[Cl^-]_i$ transient upon GABA or muscimol injections (mean ± SD, N = 3-10 mice). (J) Astrocytic $[Cl^-]_i$ trace during aCSF injection, shading indicates SD. (N = 1 mouse). (K) Change in astrocytic $[Cl^-]_i$ in response to aCSF injection (mean±SD, N = 1 mouse). (L) Duration of astrocytic $[Cl^-]_i$ change upon aCSF injection, (mean±SD, N = 1 mouse). $[Cl^-]$ = mClY -ΔF/F (%).

Discussion

In this study we found that astrocytes serve as a source of Cl^- required for sustained GABAergic transmission. We provided the first-time *in vivo* analysis of astrocytic $[Cl^-]_i$ using four imaging approaches including 2-photon, FLIM, fibre photometry, and macroscopic imaging. We show that

astrocytic $[Cl^-]_i$ *in vivo* is above the diffusion equilibrium (Figure 4), astrocytic $[Cl^-]_i$ is regulated by brain state with high $[Cl^-]_i$ during sleep and lower but highly dynamic $[Cl^-]_i$ during wakefulness (Figure 1). Astrocytic $[Cl^-]_i$ rapidly declines during neuronal activation induced by spontaneous locomotion or whisker stimulation (Figure 2) and perhaps most importantly, our observations document that astrocytic $[Cl^-]_i$ modulates neuronal activity (Figure 3). Astrocytes express $GABA_AR$s, activation of which results in Cl^- efflux that increases $[Cl^-]_o$ thus strengthening inhibitory transmission during prolonged episodes of neuronal activity. Combined, these observations show that astrocytes modulate neuronal transmission within a time-frame of seconds . Our observations support the notion that astrocytes are more tightly linked to inhibitory, than to the excitatory glutamatergic transmission in the developing and mature brain[45-49] -0.)

The role of astrocytic Cl^- in neuronal inhibition

It is well-documented that long-lasting activation of inhibitory synapses leads to a significant reduction in the amplitude of IPSPs over time, reflecting a collapse of the Cl^- gradient, due to Cl^- influx into neurons through $GABA_AR$[2,3,4]. Voltage-clamp recordings from neocortical pyramidal cells and dendrites of hippocampal CA1 pyramidal cell revealed a shift in the reversal potential of $GABA_AR$ currents during sustained inhibition signifying a decrease in transmembrane Cl^- gradient due to $[Cl^-]_o$ depletion[2,3]. Whole cell patch-clamp recordings in combination with $[Cl^-]_i$ imaging of somata of mature hippocampal CA1 pyramidal neurones, confirmed synaptically activated $GABA_AR$ mediated Cl^- accumulation[4]. Collapse of the neuronal Cl^- gradient is accelerated by pharmacological inhibition of astrocytic gap junctions in *ex vivo* brain slices. This suggests that net Cl^- extrusion from the astrocytic network might replenish $[Cl^-]_o$ during intense activation of GABAergic synapses[38]. Furthermore, recordings with Cl^- sensitive microelectrodes showed that stimulation of CA3 pyramidal neurones leads to an increase in $[Cl^-]_o$, which is reduced by applying

298 a gap junction blocker[50]. Nevertheless, $[Cl^-]_o$ in the nano-domain of synaptic clefts is unknown. We
299 here show that manipulating astrocytic $[Cl^-]_i$ by optogenetic stimulation of the Cl^- pump alleviated
300 neuronal activity during locomotion or whisker stimulation resulting in a decrease of plateau and
301 faster recovery of neuronal $[Ca^{2+}]_i$ transient. A similar potentiation of inhibitory transmission could
302 be evoked by pharmacologically activating $GABA_AR$ using the allosteric modulator of $GABA_AR$
303 diazepam (Supplemental Figure 6). Diazepam having a similar effect on neuronal activity as
304 astrocytic $[Cl^-]_i$ supports the suggestion that astrocytic $[Cl^-]_i$ modulates inhibition by $GABA_AR$
305 mediated mechanism. During optogenetic stimulation Cl^- is constantly pumped into astrocytes
306 expressing NpHR3.0 thus maintaining high astrocytic $[Cl^-]_i$ during movement or whisker
307 stimulation. When astrocytic $[Cl^-]_i$ is elevated by optogenetic stimulation the GABA-mediated Cl^-
308 efflux from astrocytes is expected to be potentiated. While NpHR3.0 is expressed throughout the
309 astrocytic membrane, as shown by 2-photon imaging, astrocytic $GABA_ARs$ are predominantly
310 expressed around the synaptic cleft[41]. Thus, Cl^- efflux is likely to occur with a high spatial precision
311 in the vicinity of inhibitory synapses[38]. Our data show that increasing astrocytic Cl^- facilitates
312 neuronal inhibition and provide the first direct evidence that astrocytic $[Cl^-]_i$ can modulate neuronal
313 activity *in vivo* (Figure 3). It is unlikely that optogenetic elevation of astrocytic $[Cl^-]_i$ altered
314 neuronal membrane potential since the photo-stimulation was not associated with changes in LFP
315 (Supplemental Figure 5). Extracellular $[Cl^-]$ is high and ranges around 130 mM. Stimulation of the
316 optogenetic Cl^- pump homogeneously distributed in astrocytes, mediates global uptake of Cl^- from
317 the extracellular space, which arguably has little impact on bulk $[Cl^-]_o$. Furthermore, Cl^- crosses the
318 blood brain barrier with ease[51]. During quiet wakefulness, activation of NpHR3.0 in astrocytes did
319 not modify spontaneous neuronal activity, suggesting that during baseline conditions, the level of
320 tonic inhibition is not affected (Supplemental Figure 5). During periods of neuronal activity release
321 of GABA from inhibitory terminals opens astrocytic $GABA_AR$[38], thus triggering local Cl^- release

into the synaptic cleft. Even though we cannot provide proof for the mechanism, we show that manipulating astrocytic $[Cl^-]_i$ consistently reduces neuronal activity during locomotion or whisker stimulation thus supporting sustained inhibition in awake behaving mice (Figure 5).

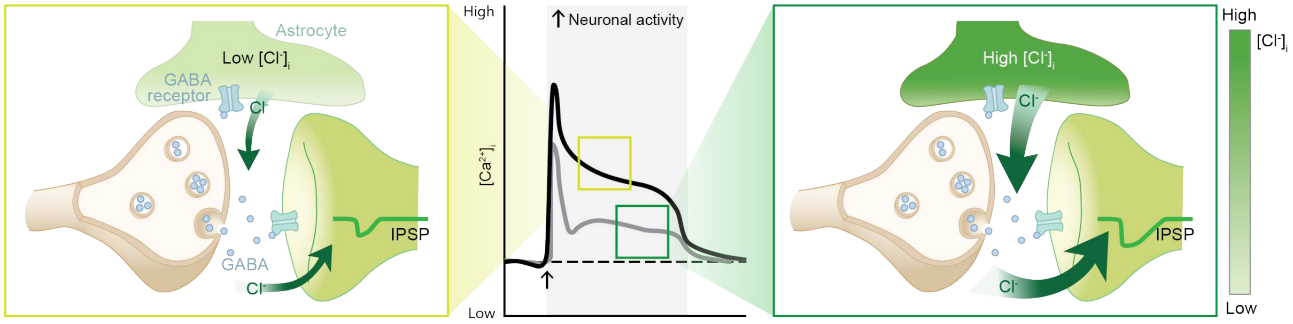

Figure 5: Astrocytic $[Cl^-]_i$ facilitates neuronal inhibition by supplying Cl^- for GABAergic synapses.

Synaptic GABA release opens $GABA_AR$ in astrocytes leading to Cl^- efflux. Astrocytic $[Cl^-]_i$ affects the duration of neural activation. Under conditions of low astrocytic $[Cl^-]_i$, neuronal activity is sustained for a longer period of time due to a reduction in the strength of GABAergic transmission over time. When astrocytic $[Cl^-]_i$ is high, activation of astrocytic $GABA_ARs$ provides an additional source of Cl^- shortening the duration of neuronal activity. The arrow indicates onset of cortical neural activity induced by spontaneous locomotion or whisker stimulation

Future perspectives

We show for the first time, that astrocytic Cl^- modulates neuronal signalling *in vivo*. These observations illuminate the importance of astrocytic Cl^- for the excitation-inhibition balance. In short, astrocytes serve as a reservoir of Cl^- that is recruited by activation of $GABA_A$ receptors of and thereby as a modulator of neuronal signalling.

Excitatory actions of GABA have been reported in about 30% of neurones from brain slices of patients with epilepsy[52] as well as *in vitro* using a variety of convulsive agents and procedures[53,54,55]. An increase of neuronal $[Cl^-]_i$ occurs after seizures, spinal cord lesions, and other pathological

conditions. Most studies investigating excitatory effects of GABA address neuronal $[Cl^-]_i$ and related regulatory mechanisms including NKCC1 and KCC2[56]. Our study highlights previously neglected contribution of astrocytic $[Cl^-]_i$ and astrocytic Cl^- conductance. Dynamic changes of $[Cl^-]$ in the synaptic cleft define the activity-dependent disinhibition, which can vary from one neuronal compartment to another or be globally regulated by astrocytes. Electrophysiological LFP recordings during manipulations of $[Cl^-]_o$ show massive increases in baseline activity, demonstrating the powerful role of $[Cl^-]_o$ in modulating neuronal activity (Supplemental Figure 5). Our data open a new avenue of research in neuroglia signalling in which a long-lasting inhibition depends on astrocytic $GABA_AR$ and astrocytic $[Cl^-]_i$. A decrease in either is expected to lower the threshold for seizure induction.

Supplemental Material:

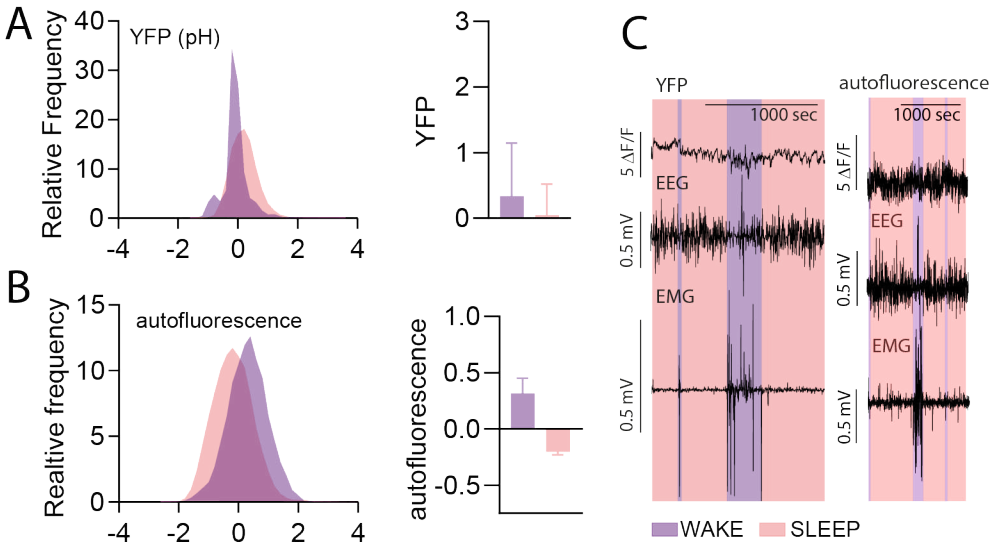

Supplemental Figure 1: In contrast to mClY, YFP or autofluorescence is not affected by brain state changes in vivo.

(A) Distribution of YFP recorded from freely moving intermittently naturally sleeping mice (N = 3 mice). YFP expressed under the *Gfap*-promotor, virally delivered into somatosensory cortex by injection. (B) Distribution of autofluorescence recorded from freely moving intermittently naturally sleeping mice, which do not express any sensor (N = 2 mice). (C) Representative traces of YFP or autofluorescence, EEG, and EMG; colour code highlights brain states sleep and awake. All fluorescent traces were inverted (-ΔF/F %).

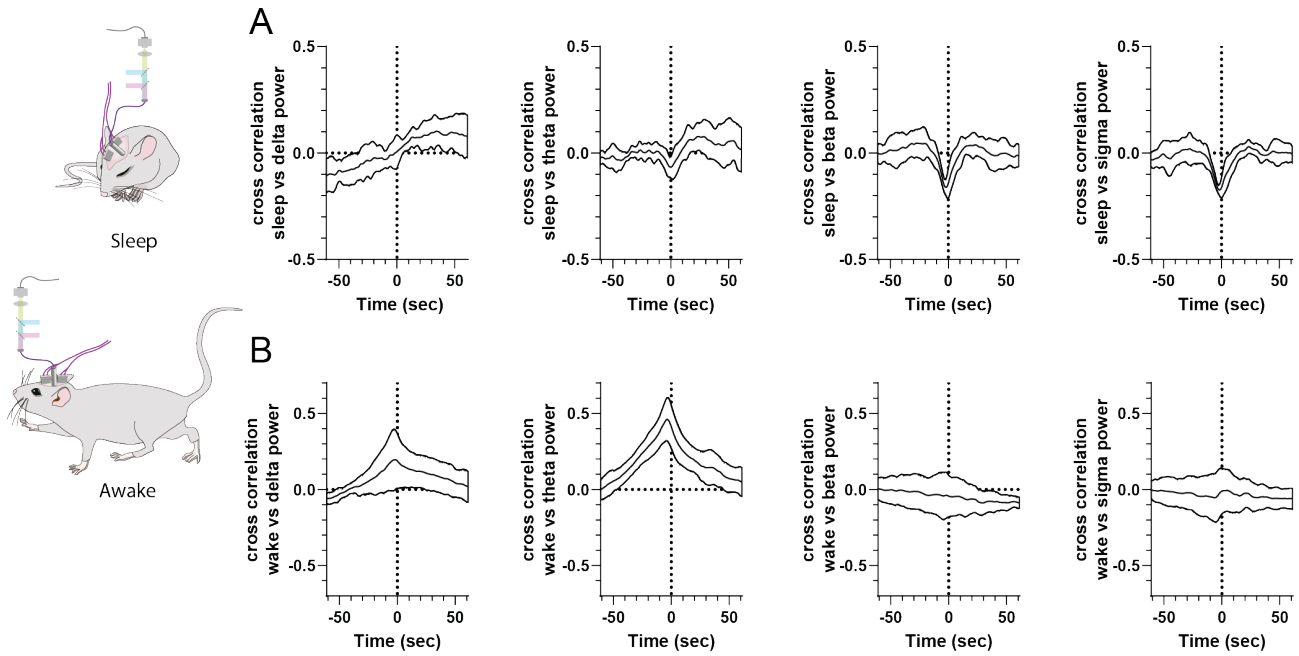

Supplemental Figure 2: Cross correlation of astrocytic $[Cl^-]_i$ and EEG power bands show a correlation between theta power and astrocytic $[Cl^-]_i$ during wakefulness with no correlation during sleep.

Cross correlation of astrocytic $[Cl^-]_i$ during sleep (A) or wakefulness (B) and EEG power bands, delta 0.2-4 Hz, theta 4-7 Hz, beta 8-15 Hz, sigma 15-30 Hz. N = 5 mice, error SD.

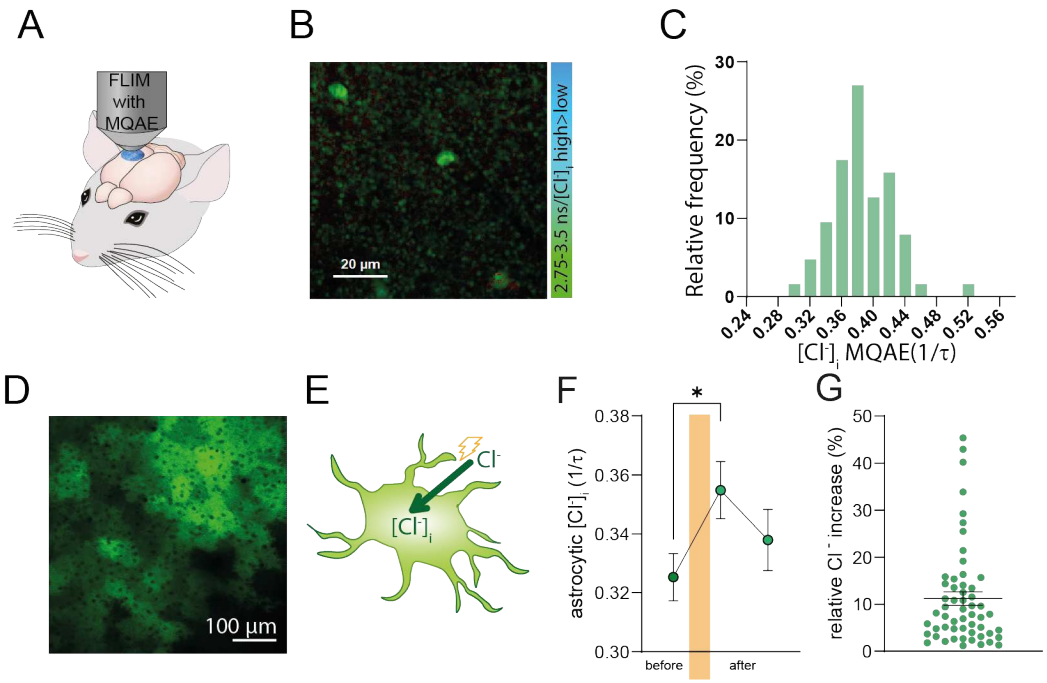

Supplemental Figure 3: Absolute $[Cl^-]_i$ using MQAE and fluorescence lifetime microscopy imaging (FLIM) in combination with optogenetic manipulation of astrocytic $[Cl^-]_i$ to significantly increase astrocytic $[Cl^-]_i$.

(A) Experimental protocol: Two-photon microscopy (2PM) fluorescence lifetime imaging (FLIM) of astrocytic $[Cl^-]_i$ using MQAE in awake head-fixed mice. (B) Representative FLIM imaged of MQAE loaded cortical astrocytes. Colour code indicates fluorescence lifetime. (C) Distribution of fluorescence lifetime (τ) determined in astrocytes representing absolute $[Cl^-]_i$ (N = 6 mice) shows a normal distribution of $[Cl^-]_i$. (D) Representative 2PM intensity imaged of NpHR3.0 expressed by cortical astrocytes. (E) The optogenetic tool NpHR3.0 is a light activated Cl^- pump, actively pumping Cl^- into astrocytes. (F) Average astrocytic $[Cl^-]_i$ upon optogenetic stimulation of NpHR3.0 is significantly increased (N = 3 mice). (G) Relative change of astrocytic $[Cl^-]_i$ upon optogenetic stimulation (N = 5 mice).

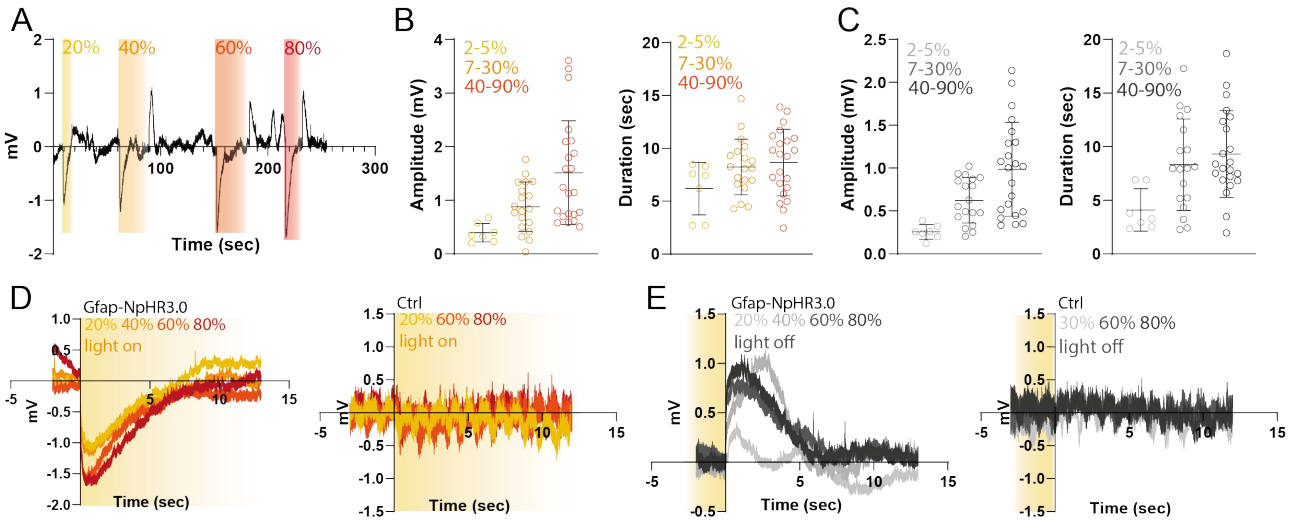

386

387 *Supplemental Figure 4: Optogenetic stimulation of astrocytes using NpHR3.0 changes $[Cl^-]_i$ in a*

388 *stimulation light intensity dependent manner.*

389 (A) Representative local field potential (LFP) of brain activity upon light stimulation with different

390 power 20, 40, 60, and 80%. (B and C) Comparison of amplitude and duration of LFP signal upon

391 activation and deactivation of light stimulation, indicate a light intensity dependent NpHR3.0

392 transport current. (D and E) Representative traces of NpHR3.0 transport current upon activation and

393 deactivation of light stimulation. And representative traces of negative control not expressing

394 NpHR3.0 upon activation and deactivation of light stimulation.

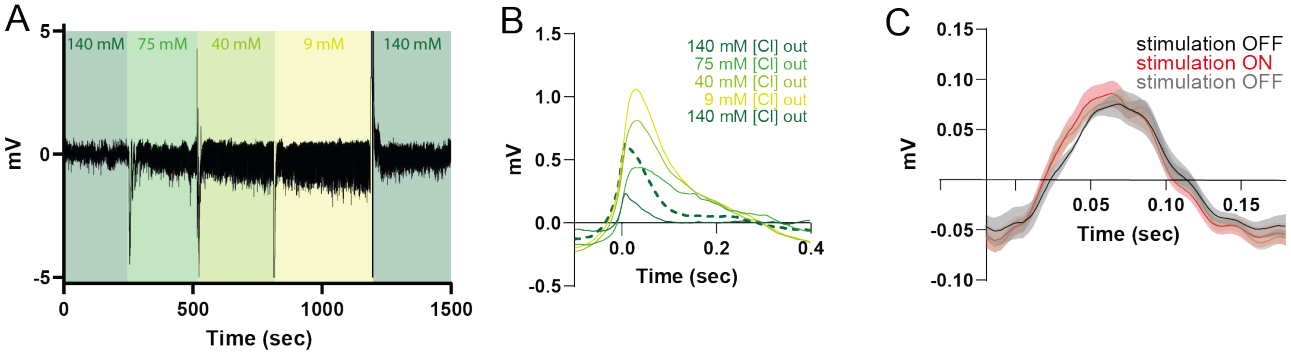

395

396 *Supplemental Figure 5: Manipulations with* $[Cl^-]_o$ *or astrocytic* $[Cl^-]_i$ *using optogenetics do not*

397 *affect spontaneous neuronal activity.*

398 (A) Representative LFP recording from the cortex with aCSF containing different $[Cl^-]$ (0, 40, 75,

399 or 140 mM), showing the impact of changed $[Cl^-]_o$ on spontaneous neuronal activity. (B) Waveform

average of LFP recorded with aCSF containing different [Cl^-]. (C) Waveform average of LFP with and without activation of NpHR3.0 in astrocytes, shows no change of spontaneous neuronal activity upon optogenetic stimulation.

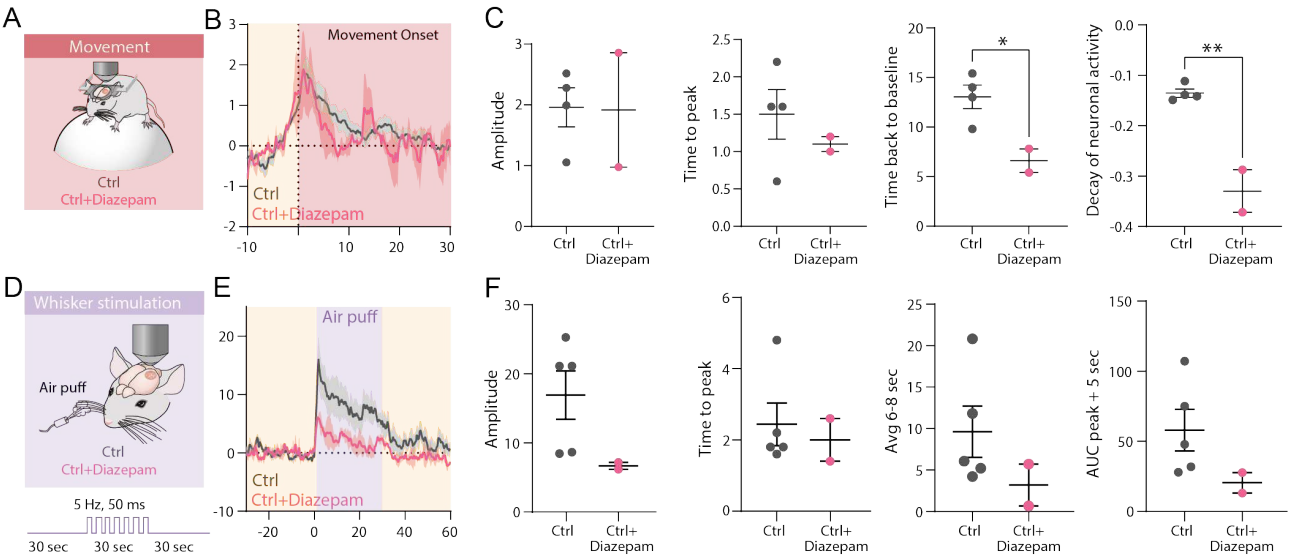

Supplemental Figure 6: $GABA_AR$ activator diazepam, which increases GABAergic inhibition, supresses the neuronal activation upon movement onset and whisker stimulation.

(A) Experimental protocol: Neuronal $[Ca^{2+}]_i$ was imaged using jRGECO expressed under the neuronal *hsyn* promoter, while pharmacologically stimulating $GABA_AR$ using diazepam. The awake, head-fixed mice were voluntarily running on a Styrofoam sphere. (B) Average neuronal $[Ca^{2+}]_i$ trace during transition from stationary to mobile, in absence and in presence of diazepam, shading indicates SEM. (N = 2-5 mice). (C) Maximal (peak) amplitude of neuronal $[Ca^{2+}]_i$ transient upon movement onset. Time to peak of neuronal $[Ca^{2+}]_i$ transient upon movement onset. Recovery time of neuronal $[Ca^{2+}]_i$ transient back to baseline (*p=0.0288, un-paired two-tailed t-test). Decay constant of neuronal $[Ca^{2+}]_i$ transient upon movement onset, (*p=0.0024, un-paired two-tailed t-test). (E) Using the same pharmacological activation of $GABA_AR$ and neuronal $[Ca^{2+}]_i$ imaging as in (A), whiskers were stimulated using air puffs. (F) Average neuronal $[Ca^{2+}]_i$ trace during whisker stimulation, while simultaneously activating the optogenetic tool NpHR3.0 in astrocytes, shading

417 indicates SEM. (N = 2-5 mice). (G) Maximal (peak) amplitude of neuronal $[Ca^{2+}]_i$ upon whisker
418 stimulation; time to peak of neuronal $[Ca^{2+}]_i$ upon whisker stimulation. Neuronal $[Ca^{2+}]_i$ during the
419 period of maximal astrocytic $[Cl^-]_i$ changes upon whisker stimulation, 6 – 8 sec after onset of
420 stimulation. Area under the curve (AUC) of neuronal $[Ca^{2+}]_i$ during 5 sec after peak.
421

Methods

Animals and surgery. This study used C57/BL6j WT mice, purchased from Janvier. Surgery was performed on mice 7 - 10 weeks old anesthetized with Isoflurane (4% induction, 1.5% maintenance) or Ketamine/Xylazine (10 mg/ml and 1 mg/ml, respectively in 0.9% saline. 0.1 ml/10 mg bodyweight i.p.). Body temperature was monitored and maintained at 37°C. **Fibre implantation.** Before fibre implantation, virus injection was performed using a 10 uL glass Hamilton syringe (NF35BV-2, Nanofil, WPI), mounted to a Nanoinjector pump (Micro4, WPI). At stereotaxic coordinates A/P: -2.53 mm, M/L: -1.5, V/D: -0.7, -0.6, -0.5 mm from bregma a concentration of $2.5*10^{11}$-$1*10^{13}$ GC/ml was injected. A glass fibre was implanted in the centre of the injection site. Two EEG electrodes were implanted via two burr wholes and two EMG wires were implanted into the next muscle. Animals were imaged 2-4 weeks after injection. **Stereotaxic AAV injections.** Virus injection was performed with the Hamilton syringe mounted to a micromanipulator (World Precision Instruments) at a 10-degree angle. At the coordinates A/P: -2.98 mm, M/L: -3.00 mm from bregma a concentration of $2.5*10^{11}$-$1*10^{13}$ GC/ml was injected. Animals were imaged 2-4 weeks after injection and after a craniotomy was performed. **Craniotomy.** A head plate was glued to the skull and a craniotomy was made above the right somatosensory cortex. After dura removal the window was sealed with a glass coverslip. For injection of pharmacological blockers during imaging an acute craniotomy was performed and covered partially with a coverslip, while the surface was kept moist with aCSF (135 mM Na^+, 142.8 mM Cl^-, 4.2 mM K^+, 1 mM Ca^{2+}, 0.8 mM Mg^{2+}, 10 mM Glucose, 10 mM HEPES). **Fluorescent dye-loading.** MQAE (1(ethoxycarbonylmethyl)26-methoxyquinolinium bromide; Sigma-Aldrich, Munich, Germany [57], 7,5 mM in aCSF) was injected via bolus loading as described before [42] and via surface loading (30 min at RT). Astrocytes are co-labeled using SR-101 surface loading (100 µM, 1 min).

Construct	Company
ssAAV-PHP.eB/2-GFAP(2.2)-mClY-WPRE-bGHp(A)	Viral Vector Facility (VVF), Neuroscience Center Zurich
ssAAV-PHP.eB/2-hGFAP(0.7)-eNpHR3.0_EGFP-WRPE-bGHp(A)	Viral Vector Facility (VVF), Neuroscience Center Zurich
AAV1-Syn-FLEX-jRGECO1a-WPRE-SV40	Penn Vector Core

pAAV5-GFAP-eGFP	Addgene

Fibre photometry. A pair of excitation LEDs (465 nm and 405 nm, Doric Lenses, Tucker Davis Technologies) were connected to a minicube (Doric Lenses) by attenuator patch cords (400-µm core, NA = 0.48, Doric Lenses). The minicube contains dichroic mirrors and clean-up filters chosen to match the excitation and emission spectra. LEDs were controlled by LED drivers (Thorlabs, Doric, Tucker Davis Technologies) and connected to a RZ-5 or RZ10-X real-time processor (Tucker-Davis Technologies). 465 nm excitation light was delivered through a patch cord to stimulate mClY or EYFP fluorescence, respectively, while 405 nm was an excitation isosbestic wavelength for mClY correcting for bleaching and signal fluctuations due to movement. 465 nm/405 nm excitation were both sinusoidally modulated at 531 Hz/211 Hz. Fiber-optic patch cords (400 µm core, NA = 0.48, Doric Lenses) provided a light path between the minicubes and the animals. Zirconia sleeves were used to attach the fibre-optic patch cords to fibre implants on the animal.

Each of the modulated signals generated by the LEDs were independently recovered using standard synchronous demodulation techniques implemented on the RZ-5/RZ10-X real-time processor (sampling rate of 1000 Hz). The commercial software Synapse (Tucker-Davis Technologies) was used to control the signal processor and was aligned to video and EEG/EMG signals through in- or outcoming TTL pulses. Files were exported for analysis to MATLAB (MathWorks). ΔF/F calculations were based on the fitted 405 nm signal or by using the median of the fluorescence signal itself.

***In vivo* macroscopic imaging.** One-photon trans-craniotomy imaging was performed on awake head fixed mice, voluntarily running on a Styrofoam sphere, or immobilized in a MAG-1 mouse holder (Narishige, Japan). A self-build microscope (Cerna, Thorlabs) equipped with a 4x objective (RMS4X-PF, Olympus) was used. Fluorescence was recorded with a cooled EMCCD camera (Andor iXon Ultra897) at indicated frame rates. jRGECO and mClY were excited using a 580 nm and 470 nm LED (CoolLED pE-4000), respectively, and filtered by a dual band filter set (ET488/561x, ET488/561rdc, Chroma). Emitted light was first filtered with a 694 nm short pass filter to block the light from the behaviour LED (FF02-694/SP-25, Semrock) and further filtered with a 500 nm (ET500LP, Chroma) and 575 nm (AT575LP) long pass filter for mCly and

jRGECO emission, respectively. Images were collected with μManager[58] (Version 2.0) and stored as 16-bit uncompressed tiff files.

***In vivo* two-photon laser scanning microscopy for Cl^- imaging.** Intensity-based two-photon chloride imaging was performed using a Galvo/Galvo scanner (Cambridge Technologies) equipped with a water-immersion 20x objective (0.95 NA, Olympus). Fluorophores were excited using a Mai Tai DeepSee laser (SpectraPhysics). Images were acquired using Sciscan software at a frame rate of 3 Hz. Emitted fluorescence was recorded with GaAsP two-channel PMT (Scientifica Chromoflex). MQAE (exλ 770 nm/ emλ bp 460/50), mClY (exλ 960 nm/ em bp 525/50), SR101 (exλ 910 nm/ em bp 595/50). **Fluorescence lifetime imaging microscopy (FLIM).** Emitted fluorescence was recorded with GaAsP hybrid photodetector connected by a light guide. TCSPC electronics and acquisition software were used for fluorescence lifetime imaging as previously described[59]. Lifetime images were analyzed using SymphoTime by fitting a bi-exponential function to the fluorescence decay. The average fluorescence lifetime of each astrocyte soma was calculated by manually drawing ROIs and averaging the values of all included pixels. All data represent mean ± SD.

Brain state tracking and sleep scoring. Mice were placed in recording chambers (ViewPoint Behavior Technology) and cables were connected to the EEG and EMG electrodes via a commutator (Plastics One, Bilaney). Mice were allowed to habituate to the recording chamber (ViewPoint Behavior Technology) for at least one day/16-24 h prior to recordings. On the day of recording, mice were connected to the fibre optic implants and recordings were performed for 2-4 hrs. EEG and EMG signals were amplified (National Instruments Inc.) and filtered (EEG signal: high-pass at 1 Hz and low-pass at 100 Hz; EMG signal: high-pass at 10 Hz and low-pass at 100 Hz), and a notch filter of 50 Hz was used to reduce power line noise. Signals were digitized using a NI USB 6343 card (National Instrument) and sampled at a sampling rate of 512 Hz. Mouse behaviour was recorded continuously using an infrared camera (Flir Systems) and used later to aid in the scoring of vigilance states. Hypnograms were created by visual inspection of EEG traces divided into 5 and subsequently 1 s epochs. Vigilance states were defined as wake (high muscle tonus and a high frequency, low amplitude EEG), NREM sleep (no muscle tonus and low frequency, high amplitude EEG,),

494 and REM sleep (no muscle tonus and high frequency, low amplitude EEG). Analysis of hypnograms was
495 done using SleepScore software (ViewPoint Behavior Technology). All data analysis was subsequently
496 performed in MATLAB using custom-made scripts.
497 **Movement tracking.** Mouse behaviour was recorded at 25 Hz with a colour CCD camera (CS165CU1/M,
498 Thorlabs) equipped with an 8 mm objective (MVL8M23, Thorlabs). During imaging the mouse was
499 illuminated with a 780 nm LED (M780L3, Thorlabs). The infra-red filter of the camera was removed.
500 Behaviour was analysed in DeepLabCut[60]. A model dataset of 1464 manually labelled frames from 14
501 individual recording sessions was used to train a ResNET-50 based network to recognize the centre of the
502 front paws.
503 **Whisker stimulation.** Neurons in the whisker barrel cortex of the right hemisphere were stimulated 10 times
504 by a series of air puffs (5 Hz, 50 ms, 20 psi) at the left side of the mouse over a time of 30 seconds with a
505 break of 60 seconds between each trial. Only trials in which the mouse was not whiskering or running during
506 the 10 seconds before stimulation started were used for analysis.
507 **Optogenetic stimulation.** Optogentic stimulation was performed using an external light source (Lumencor
508 spectra X light, spectral output 100% = 310 mW/nm) directed towards the craniotomy.
509 **Data analysis.** Fluorescence recordings were corrected for motion errors with the motion correction plugin
510 of EZcalcium[61] and post-processed in Fiji[62]. A squared ROI was selected over the area with the highest
511 intensity and the time-trace was saved. A self-written Matlab script was used to calculate the mean of the
512 whisker puff stimulation trials for each animal.
513 Motion-onset was calculated from the x and y position of the animals left front paw after DeepLabCut
514 analysis in Matlab. The moment of movement-onset was defined as an event were the front paw
515 displacement from one consecutive frame to the other was more than 150 pixels (= 6.4 mm) after a phase of
516 at least 10 seconds of still standing on the sphere. MQAE and mClY are quenched by Cl^-. The fluorescence
517 intensity is inversely correlated with surrounding [Cl^-]. Therefore, all traces recorded from mClY, MQAE,
518 YFP and autofluorescence were inverted.
519 **Drugs and pharmacology.** Drugs were diluted in aCSF. Drug were used in the following concentration:
520 GABA 500 µM, Muscimol 500 µM, Diazepam 1mg/kg i.p.

Statistics. The paired t-test or unpaired two-tailed t-test was employed to compare pairs of groups, if data passed the normality test. Otherwise, the Wilcoxon matched-pairs signed rank test or Mann-Whitney test was used for comparison. * $p < 0.05$, ** $p < 0.005$, *** $p < 0.001$, **** $p < 0.0001$.

References

1 Misgeld, U., Deisz, R. A., Dodt, H. U. & Lux, H. D. The role of chloride transport in postsynaptic inhibition of hippocampal neurons. *Science* **232**, 1413-1415, doi:10.1126/science.2424084 (1986).

2 Staley, K. J. & Proctor, W. R. Modulation of mammalian dendritic GABA(A) receptor function by the kinetics of Cl- and HCO3- transport. *The Journal of physiology* **519 Pt 3**, 693-712, doi:10.1111/j.1469-7793.1999.0693n.x (1999).

3 Staley, K. J., Soldo, B. L. & Proctor, W. R. Ionic mechanisms of neuronal excitation by inhibitory GABAA receptors. *Science* **269**, 977-981, doi:10.1126/science.7638623 (1995).

4 Isomura, Y. *et al.* Synaptically activated Cl- accumulation responsible for depolarizing GABAergic responses in mature hippocampal neurons. *Journal of neurophysiology* **90**, 2752-2756, doi:10.1152/jn.00142.2003 (2003).

5 Verkhratsky, A. & Nedergaard, M. Physiology of Astroglia. *Physiological reviews* **98**, 239-389, doi:10.1152/physrev.00042.2016 (2018).

6 Eggermann, E., Kremer, Y., Crochet, S. & Petersen, C. C. H. Cholinergic signals in mouse barrel cortex during active whisker sensing. *Cell Rep* **9**, 1654-1660, doi:10.1016/j.celrep.2014.11.005 (2014).

7 Polack, P. O., Friedman, J. & Golshani, P. Cellular mechanisms of brain state-dependent gain modulation in visual cortex. *Nat Neurosci* **16**, 1331-1339, doi:10.1038/nn.3464 (2013).

8 Schiemann, J. *et al.* Cellular mechanisms underlying behavioral state-dependent bidirectional modulation of motor cortex output. *Cell Rep* **11**, 1319-1330, doi:10.1016/j.celrep.2015.04.042 (2015).

9 Ding, F. *et al.* Changes in the composition of brain interstitial ions control the sleep-wake cycle. *Science* **352**, 550-555, doi:10.1126/science.aad4821 (2016).

10 Rasmussen, R., Jensen, M. H. & Heltberg, M. L. Chaotic Dynamics Mediate Brain State Transitions, Driven by Changes in Extracellular Ion Concentrations. *Cell Syst* **5**, 591-603 e594, doi:10.1016/j.cels.2017.11.011 (2017).

11 Rasmussen, R. *et al.* Cortex-wide Changes in Extracellular Potassium Ions Parallel Brain State Transitions in Awake Behaving Mice. *Cell Rep* **28**, 1182-1194 e1184, doi:10.1016/j.celrep.2019.06.082 (2019).

12 Cirelli, C. The genetic and molecular regulation of sleep: from fruit flies to humans. *Nature reviews. Neuroscience* **10**, 549-560, doi:10.1038/nrn2683 (2009).

13 Cirelli, C. *et al.* Reduced sleep in Drosophila Shaker mutants. *Nature* **434**, 1087-1092, doi:10.1038/nature03486 (2005).

14 Tatsuki, F. *et al.* Involvement of Ca(2+)-Dependent Hyperpolarization in Sleep Duration in Mammals. *Neuron* **90**, 70-85, doi:10.1016/j.neuron.2016.02.032 (2016).

15 Yoshida, K. *et al.* Leak potassium channels regulate sleep duration. *Proceedings of the National Academy of Sciences of the United States of America* **115**, E9459-E9468, doi:10.1073/pnas.1806486115 (2018).

16 Balestrino, M., Aitken, P. G. & Somjen, G. G. The effects of moderate changes of extracellular K+ and Ca2+ on synaptic and neural function in the CA1 region of the hippocampal slice. *Brain research* **377**, 229-239, doi:10.1016/0006-8993(86)90863-2 (1986).

17 Brocard, F. *et al.* Activity-dependent changes in extracellular Ca2+ and K+ reveal pacemakers in the spinal locomotor-related network. *Neuron* **77**, 1047-1054, doi:10.1016/j.neuron.2013.01.026 (2013).

18 Frohlich, F., Bazhenov, M., Iragui-Madoz, V. & Sejnowski, T. J. Potassium dynamics in the epileptic cortex: new insights on an old topic. *The Neuroscientist : a review journal bringing neurobiology, neurology and psychiatry* **14**, 422-433, doi:10.1177/1073858408317955 (2008).

19 Octeau, J. C. *et al.* Transient, Consequential Increases in Extracellular Potassium Ions Accompany Channelrhodopsin2 Excitation. *Cell Rep* **27**, 2249-2261 e2247, doi:10.1016/j.celrep.2019.04.078 (2019).

20 Poolos, N. P., Mauk, M. D. & Kocsis, J. D. Activity-evoked increases in extracellular potassium modulate presynaptic excitability in the CA1 region of the hippocampus. *Journal of neurophysiology* **58**, 404-416, doi:10.1152/jn.1987.58.2.404 (1987).

21 Shih, P. Y. *et al.* Retrograde synaptic signaling mediated by K+ efflux through postsynaptic NMDA receptors. *Cell Rep* **5**, 941-951, doi:10.1016/j.celrep.2013.10.026 (2013).

22 Tong, X. *et al.* Astrocyte Kir4.1 ion channel deficits contribute to neuronal dysfunction in Huntington's disease model mice. *Nat Neurosci* **17**, 694-703, doi:10.1038/nn.3691 (2014).

23 Wang, F., Xu, Q., Wang, W., Takano, T. & Nedergaard, M. Bergmann glia modulate cerebellar Purkinje cell bistability via Ca2+-dependent K+ uptake. *Proceedings of the National Academy of Sciences of the United States of America* **109**, 7911-7916, doi:10.1073/pnas.1120380109 (2012).

24 Bazhenov, M., Timofeev, I., Steriade, M. & Sejnowski, T. J. Potassium model for slow (2-3 Hz) in vivo neocortical paroxysmal oscillations. *Journal of neurophysiology* **92**, 1116-1132, doi:10.1152/jn.00529.2003 (2004).

25 Krishnan, G. P., Gonzalez, O. C. & Bazhenov, M. Origin of slow spontaneous resting-state neuronal fluctuations in brain networks. *Proceedings of the National Academy of Sciences of the United States of America* **115**, 6858-6863, doi:10.1073/pnas.1715841115 (2018).

26 Thompson, S. M. & Gahwiler, B. H. Activity-dependent disinhibition. I. Repetitive stimulation reduces IPSP driving force and conductance in the hippocampus in vitro. *Journal of neurophysiology* **61**, 501-511, doi:10.1152/jn.1989.61.3.501 (1989).

27 Bekar, L. K. & Walz, W. Intracellular chloride modulates A-type potassium currents in astrocytes. *Glia* **39**, 207-216, doi:10.1002/glia.10096 (2002).

28 Bevensee, M. O., Apkon, M. & Boron, W. F. Intracellular pH regulation in cultured astrocytes from rat hippocampus. II. Electrogenic Na/HCO3 cotransport. *J Gen Physiol* **110**, 467-483 (1997).

29 Kettenmann, H., Backus, K. H. & Schachner, M. gamma-Aminobutyric acid opens Cl-channels in cultured astrocytes. *Brain research* **404**, 1-9 (1987).

30 Kimelberg, H. K. Active accumulation and exchange transport of chloride in astroglial cells in culture. *Biochimica et biophysica acta* **646**, 179-184 (1981).

31 Smith, Q. R., Johanson, C. E. & Woodbury, D. M. Uptake of 36Cl and 22Na by the brain-cerebrospinal fluid system: comparison of the permeability of the blood-brain and blood-cerebrospinal fluid barriers. *Journal of neurochemistry* **37**, 117-124 (1981).

32 Walz, W. & Mukerji, S. KCl movements during potassium-induced cytotoxic swelling of cultured astrocytes. *Experimental neurology* **99**, 17-29 (1988).

33 Untiet, V. *et al.* Glutamate transporter-associated anion channels adjust intracellular chloride concentrations during glial maturation. *Glia* **65**, 388-400, doi:10.1002/glia.23098 (2017).

34 Engels, M. *et al.* Glial Chloride Homeostasis Under Transient Ischemic Stress. *Frontiers in cellular neuroscience* **15**, 735300, doi:10.3389/fncel.2021.735300 (2021).

35 von Blankenfeld, G. & Kettenmann, H. Glutamate and GABA receptors in vertebrate glial cells. *Molecular neurobiology* **5**, 31-43, doi:10.1007/bf02935611 (1991).

36 Bormann, J. & Kettenmann, H. Patch-clamp study of gamma-aminobutyric acid receptor Cl- channels in cultured astrocytes. *Proceedings of the National Academy of Sciences of the United States of America* **85**, 9336-9340 (1988).

37 MacVicar, B. A., Tse, F. W., Crichton, S. A. & Kettenmann, H. GABA-activated Cl- channels in astrocytes of hippocampal slices. *The Journal of neuroscience : the official journal of the Society for Neuroscience* **9**, 3577-3583 (1989).

38 Egawa, K., Yamada, J., Furukawa, T., Yanagawa, Y. & Fukuda, A. Cl(-) homeodynamics in gap junction-coupled astrocytic networks on activation of GABAergic synapses. *The Journal of physiology* **591**, 3901-3917, doi:10.1113/jphysiol.2013.257162 (2013).

39 Zhong, S., Navaratnam, D. & Santos-Sacchi, J. A genetically-encoded YFP sensor with enhanced chloride sensitivity, photostability and reduced ph interference demonstrates augmented transmembrane chloride movement by gerbil prestin (SLC26a5). *PloS one* **9**, e99095, doi:10.1371/journal.pone.0099095 (2014).

40 Vanderwolf, C. H. Hippocampal Electrical Acitvity and Voluntary Movement in Rat. *Electroen Clin Neuro* **26**, 407-+, doi:Doi 10.1016/0013-4694(69)90092-3 (1969).

41 Riquelme, R., Miralles, C. P. & De Blas, A. L. Bergmann glia GABA(A) receptors concentrate on the glial processes that wrap inhibitory synapses. *The Journal of neuroscience : the official journal of the Society for Neuroscience* **22**, 10720-10730 (2002).

42 Kovalchuk, Y. & Garaschuk, O. Two-photon chloride imaging using MQAE in vitro and in vivo. *Cold Spring Harbor protocols* **2012**, 778-785, doi:10.1101/pdb.prot070037 (2012).

43 Rasmussen, R., Nedergaard, M. & Petersen, N. C. Sulforhodamine 101, a widely used astrocyte marker, can induce cortical seizure-like activity at concentrations commonly used. *Scientific reports* **6**, 30433, doi:10.1038/srep30433 (2016).

44 Delekate, A. *et al.* Metabotropic P2Y1 receptor signalling mediates astrocytic hyperactivity in vivo in an Alzheimer's disease mouse model. *Nature communications* **5**, 5422, doi:10.1038/ncomms6422 (2014).

45 Kang, J., Jiang, L., Goldman, S. A. & Nedergaard, M. Astrocyte-mediated potentiation of inhibitory synaptic transmission. *Nat Neurosci* **1**, 683-692, doi:10.1038/3684 (1998).

46 Matos, M. *et al.* Astrocytes detect and upregulate transmission at inhibitory synapses of somatostatin interneurons onto pyramidal cells. *Nature communications* **9**, 4254, doi:10.1038/s41467-018-06731-y (2018).

47 Kaczor, P., Rakus, D. & Mozrzymas, J. W. Neuron-astrocyte interaction enhance GABAergic synaptic transmission in a manner dependent on key metabolic enzymes. *Frontiers in cellular neuroscience* **9**, 120, doi:10.3389/fncel.2015.00120 (2015).

48 Takano, T. *et al.* Chemico-genetic discovery of astrocytic control of inhibition in vivo. *Nature* **588**, 296-302, doi:10.1038/s41586-020-2926-0 (2020).

49 Mederos, S. *et al.* GABAergic signaling to astrocytes in the prefrontal cortex sustains goal-directed behaviors. *Nat Neurosci* **24**, 82-92, doi:10.1038/s41593-020-00752-x (2021).

50 Kroeger, D., Tamburri, A., Amzica, F. & Sik, A. Activity-dependent layer-specific changes in the extracellular chloride concentration and chloride driving force in the rat hippocampus. *Journal of neurophysiology* **103**, 1905-1914, doi:10.1152/jn.00497.2009 (2010).

51 Hladky, S. B. & Barrand, M. A. Fluid and ion transfer across the blood-brain and blood-cerebrospinal fluid barriers; a comparative account of mechanisms and roles. *Fluids Barriers CNS* **13**, 19, doi:10.1186/s12987-016-0040-3 (2016).

52 Cohen, I., Navarro, V., Clemenceau, S., Baulac, M. & Miles, R. On the origin of interictal activity in human temporal lobe epilepsy in vitro. *Science* **298**, 1418-1421, doi:10.1126/science.1076510 (2002).

53 Dzhala, V. I. & Staley, K. J. Excitatory actions of endogenously released GABA contribute to initiation of ictal epileptiform activity in the developing hippocampus. *The Journal of neuroscience : the official journal of the Society for Neuroscience* **23**, 1840-1846 (2003).

54 Yamada, J. *et al.* Cl- uptake promoting depolarizing GABA actions in immature rat neocortical neurones is mediated by NKCC1. *The Journal of physiology* **557**, 829-841, doi:10.1113/jphysiol.2004.062471 (2004).

55 Quilichini, P. P. *et al.* Effects of antiepileptic drugs on refractory seizures in the intact immature corticohippocampal formation in vitro. *Epilepsia* **44**, 1365-1374, doi:10.1046/j.1528-1157.2003.19503.x (2003).

56 Ben-Ari, Y., Khalilov, I., Kahle, K. T. & Cherubini, E. The GABA excitatory/inhibitory shift in brain maturation and neurological disorders. *The Neuroscientist : a review journal bringing neurobiology, neurology and psychiatry* **18**, 467-486, doi:10.1177/1073858412438697 (2012).
57 Verkman, A. S. Development and biological applications of chloride-sensitive fluorescent indicators. *Am J Physiol* **259**, C375-388 (1990).
58 Edelstein, A. D. *et al.* Advanced methods of microscope control using muManager software. *J Biol Methods* **1**, doi:10.14440/jbm.2014.36 (2014).
59 Kaneko, H., Putzier, I., Frings, S., Kaupp, U. B. & Gensch, T. Chloride accumulation in mammalian olfactory sensory neurons. *The Journal of neuroscience : the official journal of the Society for Neuroscience* **24**, 7931-7938, doi:10.1523/JNEUROSCI.2115-04.2004 (2004).
60 Nath, T. *et al.* Using DeepLabCut for 3D markerless pose estimation across species and behaviors. *Nature protocols* **14**, 2152-2176, doi:10.1038/s41596-019-0176-0 (2019).
61 Cantu, D. A. *et al.* EZcalcium: Open-Source Toolbox for Analysis of Calcium Imaging Data. *Front Neural Circuits* **14**, 25, doi:10.3389/fncir.2020.00025 (2020).
62 Schindelin, J. *et al.* Fiji: an open-source platform for biological-image analysis. *Nature methods* **9**, 676-682, doi:10.1038/nmeth.2019 (2012).